Heat and Mass Transfer 35 (1999) 205–211 © Springer-Verlag 1999

Critical flow with high pressure water flowing in small diameter sharp-edged tubes

J. Xu, R. Wang

Abstract The transient critical flow experiment was carried out in the high-pressure test loop. The break sections were the sharp-edged tubes with inner diameter of nearly 4 mm but with quite different lengths. The initial pressure was up to 22.0 MPa and the inlet subcooling covered the range of 0 to 60°C. New critical flow data were provided and the effects of inlet liquid subcooling and tube lengths were described. The proposed empirical nonequilibrium correlation was used to calculate the critical mass flow rate for such small diameter tube.

List of symbols

C	pressure floss coefficient at the sharp-edged entrance region
D	tube inside diameter, m
G	critical mass velocity, kg/m^{2}s
L	total length of the sharp-edged tube, m
N	thermal nonequilibrium coefficient defined as the true vapour mass fraction divided by the equilibrium vapour mass fraction
P_c	critical pressure measured upstream 0.5 mm of the exit plane
P_o	upstream pressure, Pa
P_t	pressure at the minimum cross section at the tube entrance region, Pa
$P_{sat}(T_o)$	saturated pressure corresponding to the upstream temperature T_o, Pa
s_o	upstream liquid entropy, J/kg °C
$s_g(P_c)$	saturated vapour entropy corresponding to P_c
$s_l(P_c)$	saturated liquid entropy corresponding to P_c
T_c	critical temperature, K
v_{gc}	vapour specific volume at the choking plane, m^3/kg
v_{lo}	upstream liquid specific volume, m^3/kg
x_c	vapour true mass fraction at the choking plane
x_e	vapour equilibrium mass fraction at the choking plane
ΔP_a	acceleration pressure loss across the tube, Pa
ΔT_{sub}	upstream liquid subcooling, °C
ρ_l	liquid density, kg/m^3
η	critical pressure ratio defined as the critical pressure divided by the upstream pressure

Received on 9 September 1998

J. Xu
R. Wang
Hemispheric Center for Environmental Technology
Florida International University
Miami, FL33174, USA

Correspondence to: J. Xu

Introduction

Two-phase critical flow is formed when the liquid discharges from the relative high pressure containers to the low pressure environment. Such phenomenon has been found vide range of applications, such as in the field of nuclear power plant, boilers and chemical engineering, and has been given great attention in the past years. However, experimental investigation on the two-phase critical flow was mainly conducted under the condition of low pressure and for longer tube geometry. This is because the high-pressure critical flow experiment requires much expensive facility and running cost. Table 1 summarizes the experimental studies available in the published literature. The available two-phase critical flow data mainly concentrates on the low pressure and long tubes. The critical data at high-pressure is very scarce.

In addition to the experimental work, many jobs have also been done in the theoretical analysis of the critical flow. Especially in recent years, the phenomenon of flashing flow has been studied in relation to the critical flow problem [11–15]. Models that account for thermal nonequilibrium for initially saturated or subcooled states must represent the physics of the nucleation process and the growth of bubbles in a transient pressure environment. These models require a great deal of information to complete the model description such as nucleation site density, bubble diameter, interphase friction characteristics and heat transfer, and criteria that account for different flow regimes. The disadvantage of such models is that some parameters should be assumed to fit the experiment data, and the calculation needs much computer time.

The aim of this paper is to obtain the critical flow data at high pressure, and to study how the inlet liquid subcooling and tube geometry affect the critical flow. Based on the experimental data, a correlation was proposed to calculate the critical flow mass velocity, which emphasized the thermal nonequilibrium between the two phases.

Experiment

The transient critical flow experiment was conducted in the high-pressure steam water loop. The main objective was to investigate the system transition characteristics and obtain the critical flow database. Figure 1 illustrated the test system. The feed water was pressurized by a plunge

Table 1.

Authors	Parameters	Entrance form	Tube diameter	Tube length	L/D	Argument
Isbin et al. [1]	$P_c = 0.28$ to 3 bar, $x_c = 0.01$ to 1.0	conical	9.5 to 26.5 mm	610 mm	23 to 64	Exit pressure was not measured exactly
Fauske [2]	$P_c = 3$ to 25 bar, $x_c = 0.01$ to 0.7	conical	3.2 to 12.3 mm	1429 to 2794 mm	116 to 873	
Zaloudek [3]	$P_c = 2.76$ to 7.58 bar, $x_c = 0.004$ to 0.99	conical	13.2 to 15.9 mm	610 to 1219 mm	38 to 92	Exit pressure was not measured exactly
Faletti [4]	$P_c = 1.72$ to 5.52 bar, $x_c = 0.001$ to 0.96	conical	5 and 9.8 mm	229 to 893 mm	23 to 178	Annular test section, D is the mean hydraulic diameter
James [5]	$P_c = 1$ to 4.4 bar, $H_o = 535$ to 2790 kJ/kg	Not reported	16 to 203 mm	3658 mm	18 to 48	Upstream pressure was not given
Zaloudek [6]	$P_o = 8$ to 25 bar initially subcooling water	Sharp-edged entrance	6.35 to 15.9 mm	0.8 to 127 mm	0.05 to 20	Both effects of Non-equilibrium and non condensable gas are important
Zaloudek [7]	$P_o = 27.6$ to 124 bar, $H_o =$ 976 to 1239 kJ/kg	conical	12.8 mm	254 mm	20	Non-equilibrium effect is important
Fauske [8]	$P_o = 7$ to 24 bar, saturated water	Sharp-edged entrance	6.35 mm	0 to 254 mm	0 to 40	Non-equilibrium effect is important
Sozzi & Sutherland [9]	$P_o = 41$ to 69 bar, $T_o = 232$ to 288°C	Radiused entry	12.7 mm	0 to 1775 mm	0 to 140 mm	Non-equilibrium effect is important when $L/D < 10$
Hutcherson [10] vessel bottom discharging test	$P_o = 20$ to 27.6 bar saturated water	conical	108 mm	324 mm	3	Non-equilibrium effect is important

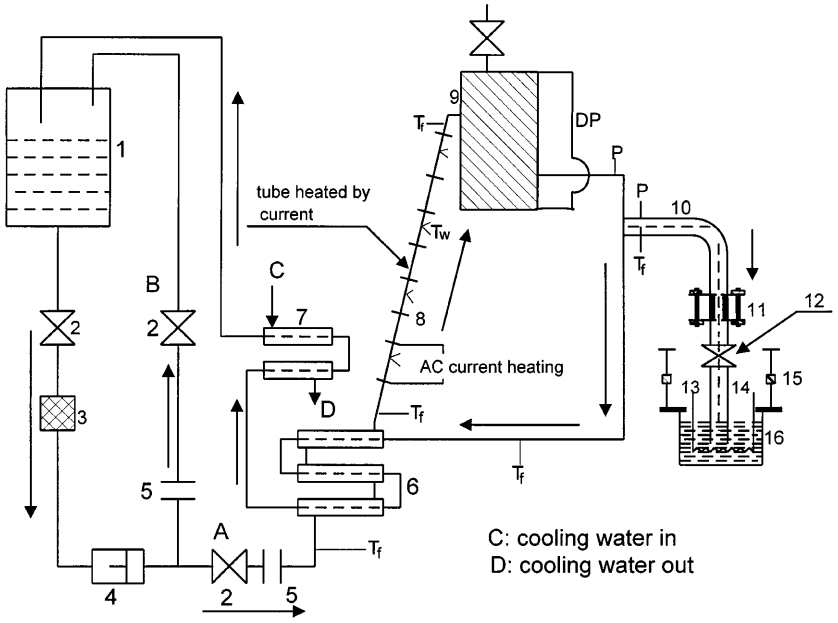

Fig. 1. Transient critical flow experimental loop *1* Water tank; *2* Control valve; *3* Filter; *4* High pressure plunger pump; *5* Orifice; *6* Regenerative heat exchanger; *7* Heat exchanger; *8* Electrode; *9* Pressure vessel; *10* Connection tube upstream of the break nozzle; *11* Break tube section unit; *12* Shutoff valve; *13* Coiled copier heat exchanger; *14* Expansion tube; *15* Load cell; *16* Water collection tank

pump and was separated into two circuits, one passing through the bypass to adjust the pressure and the loop mass flow rate, and the other flowing through orifices and then into a heated section with the inner diameter of 16.0 mm. The fluid out of the heated tube, which has a controlled subcooling, entered the pressure vessel, which has a volume of 0.125 m^3. The controlled subcooling water exited the bottom of the pressure vessel through a tube with an inner diameter of 30.0 mm. The break test section, also shown in Fig. 1, mainly consisted of the sharp-edged tubes and a shutoff gate valve. When the main circuit was operated under the conditions of a controlled system pressure, flow rate and subcooling of the fluid entering the pressure vessel, the shutoff gate valve was opened suddenly. The total time for the gate valve from fully close to fully open was less than 0.5 s. The hot water then discharged through the break test section, entered a short expansion tube with the inner diameter of 20.0 mm, and

was collected in a catch tank. In order to cool the mixture in the catch tank, a coiled copper heat exchanger was inserted in the catch tank. The catch tank was supported vertically on two lugs through the two load cells. By use of the two load cells, the time dependent mass of the catch tank could be measured, from which we could acquire the discharge flow rate through the break section.

Initially, by adjusting valves A and B, the desired system pressure P_o and main circuit flow rate m_o could be obtained. By adjusting the alternating current power supplied at the heating tube at the given mass flow rate, we could obtain the desired subcooling, ΔT_{sub} of the fluid entering the pressure vessel. Under the conditions of steady operation, the shutoff gate valve was opened suddenly.

The mass flow rate of the main circuit was measured by two orifices before the fluid entered the regenerative heat exchanger. The fluid temperatures were measured by the NiCr-NiSi jacket thermocouples along the heated tube and at the inlet and outlet of the pressure vessel. The differential pressure transducer was installed between the top and the bottom of the pressure vessel to determine the liquid level during the discharge period. The pressure gauges were set along the break section tube, upstream and downstream of the break tube. For each break tube, a pressure transducer was installed at 0.5 mm upstream of tube exit, this pressure was treated as the tube exit pressure (also called as the critical pressure from the engineering purpose). Fluid temperatures were measured by NiCr-NiSi jacket thermocouples. The uncertainties of the pressures and temperatures were ± 0.05 MPa (relative error was 1.6%) and $\pm 1°C$, respectively. The error of the discharge mass measurement was within $\pm 0.98\%$. All electric signals were transferred to IBM 486 computer through an IMP 3595 C high quality data collector (England).

Conceptually, the tank mass measurements obtained from two load cells were differentiated with respect to time. This yielded the mass flow rate directly. The slop of the resulting test fit line was taken to be the mass flow rate. This method is dependent on the assumption that the flow is quasi-static. For time less than 1–2 s after the gate valve opening at the very early age of discharge, this method may introduce an error into the mass flow rate, the maximum error estimated to be 6% in this short period. After this early discharge period, the mass flow rate error is estimated to be 0.98%.

The break sections were the sharp-edged tubes, with the inside diameter nearly of 4.0 mm (each tube diameter was measured by optical method) but with different lengths. Their dimensions were summarized in the following table.

Table 2. Break section dimensions

	L (mm)	D (mm)	L/D
No. 1	4.0	4.05	0.99
No. 2	20.0	4.03	4.96
No. 3	39.3	4.06	9.68
No. 4	65.0	4.03	16.13
No. 5	99.1	3.87	25.61

Experiment results and correlation

Two-phase critical flow is a complicated phenomenon. It not only depends on the upstream physical properties, but also on the channel geometry. Early empirical nonequilibrium model presented by Henry [16] is only suitable for long tubes with L/D larger than 12.

Figure 2 shows critical flow rates versus inlet pressure at inlet saturated condition. Critical flow rates rise with increasing the inlet pressure, but decrease with increasing the tube length to diameter ratio L/D. The effect of inlet subcooling on the mass flow rate at two different inlet pressures were shown in Figs. 3 and 4, respectively. The following conclusions can be drawn from these two figures.

- For orifices or very short tubes, critical flow rates only get slow increase with increasing the inlet subcooling. For such short channels, the time of liquid passing through the channels is very short. Thus the liquid flashing when the liquid passes through the orifices can be neglected. The critical mass flow rates are mainly relied on the inlet pressure.
- For longer tubes, critical mass flow rates rise with increasing the inlet subcooling at lower inlet subcooling

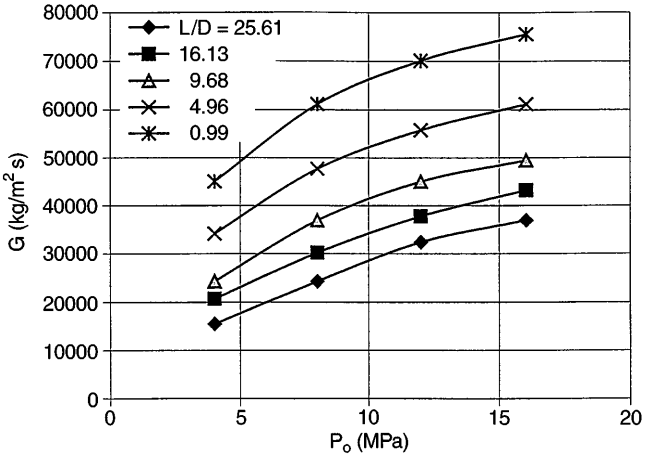

Fig. 2. Critical mass velocity versus upstream pressure

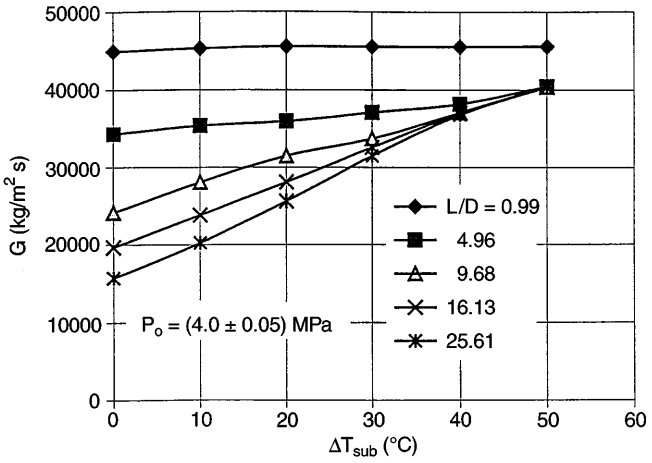

Fig. 3. Critical mass velocity versus upstream liquid subcooling

(e.g. $\Delta T_{sub} < 30 \sim 40°C$). However, such mass flow rates get very slow rise at higher inlet subcooling.
- For longer tubes (e.g. $L/D > 4.96$) and higher inlet subcooling, critical mass flow rates nearly get the constant values.

In order to develop a nonequilibrium critical flow rate correlation, the authors gave the following assumption and the corresponding flow pattern was shown in Fig. 5. Generally, the flow is divided into two regions. One is the liquid jet entrance region, and the other is the nonequilibrium two phase region.

The liquid is flowing and entering the tube entrance from the upstream stationary state in the form of liquid jet. The true flow cross section area is decreased, obtains a minimum area at $z = z_t$ and then increases until the jet reaches the full tube cross section at $z = z_f$. The pressure drop from $z = 0$ to $z = z_t$ is

$$P_o - P_t = \frac{G^2 v_{lo}}{2C^2} \tag{1}$$

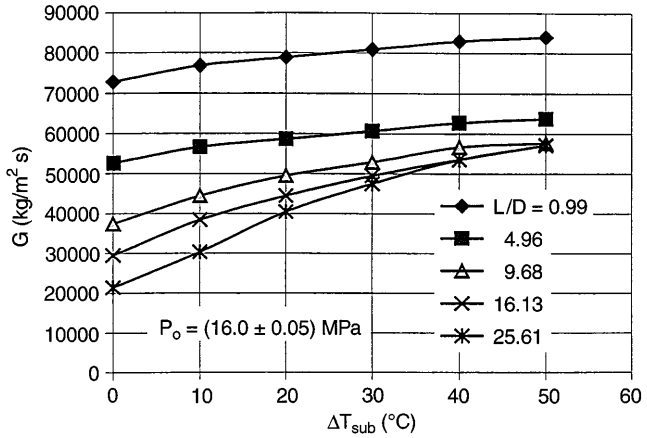

Fig. 4. Critical mass velocity versus upstream liquid subcooling

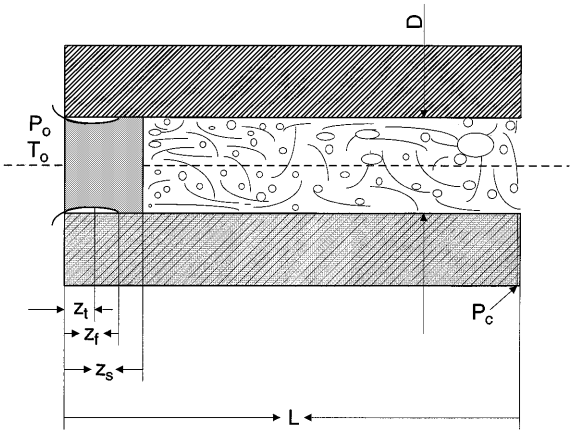

Fig. 5. Two phase critical flow in sharp-edged tubes for saturated or subcooled inlet condition Z_t: the axial distance where the minimal area across section of the liquid jet is; Z_f: the axial distance where the liquid jet is full of the whole tube; Z_s: the axial distance where the liquid has a certain superheat and the flashing begins; P_c: exit pressure

where C is the entrance coefficient and gets the value of 0.61, v_{lo} the inlet liquid specific volume.

At somewhere downstream of the location $z = z_f$, the liquid pressure decrease leads to a certain liquid superheat ΔT_{sup}, which causes the liquid flashing occurred. The value of ΔT_{sup} at which the flashing begins is very difficult to determine. It is depended on the decompression rate, the quantity of noncondensible gas and so on.

From the flashing inception location $z = z_s$ to the exit of the tube, the nonequilibrium two-phase flow exists in the tube. The present report gives the following assumption: the friction pressure drop is neglected and the homogenous flow exists in the tube. The acceleration pressure drop due to the vapour quality increase was

$$\Delta P_a = G^2 x_c (v_{gc} - v_{lo}) \tag{2}$$

where v_{gc} is the vapour specific volume and x_c the true vapour mass fraction at tube exit.

Thus the total pressure drop across the tube section is

$$P_o - P_c = G^2 \left(\frac{v_{lo}}{2C^2} + x_c (v_{gc} - v_{lo}) \right) \tag{3}$$

Based on Eq. (3), once the tube exit pressure P_c, and the corresponding true vapour mass fraction x_c are determined, the critical mass flow rate can be obtained at the given upstream pressure and temperature. The critical pressure ratio η is defined by the exit pressure divided by the upstream pressure ($\eta = P_c/P_o$). Figure 6 shows η versus the tube length to tube diameter ratio L/D. Also shown in Fig. 6 includes the data of Fauske [2]. For longer tubes whose lengths are 12 times larger than diameters, η nearly does not change. Based on this figure, η can be correlated as

$$\begin{aligned} \eta &= 0.17 + 0.155 \operatorname{Log}_e (L/D) \qquad L/D \le 12 \\ &= 0.55 \qquad\qquad\qquad\qquad\quad L/D > 12 \end{aligned} \tag{4}$$

Now the next job concerns on the true exit vapour mass fraction x_c. The liquid entropy in the stationary state of (P_o, T_o) is s_o. The exit equilibrium vapour mass fraction x_e is

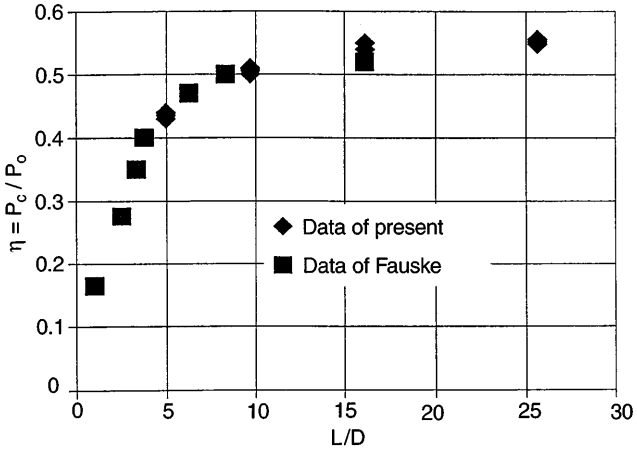

Fig. 6. Critical pressure ratio versus L/D

$$x_e = \frac{s_o - s_l(P_c)}{s_g(P_c) - s_l(P_c)} \tag{5}$$

where $s_g(P_c)$ and $s_l(P_c)$ are the saturated vapor and liquid entropies at the exit pressure P_c.

Generally the exit true vapour mass fraction is less than the equilibrium value due to the nonequilibrium between the two phases. In this paper, N, the nonequilibrium coefficient number, is defined as the ratio of exit true mass fraction to that of equilibrium value. The value of N shows that the degree at which the flow approaches the thermal equilibrium. When N approaches zero, the flow shows the "frozen flow" characteristics. On the other hand, the liquid-vapor two phases get equilibrium state when N is set to be unity. At the given upstream state (P_o, T_o), the ratio of L/D and the measured critical mass velocity G, x_c is calculated from Eq. (3), and the equilibrium value x_e is calculated from Eq. (5). With x_c divided by x_e obtains the thermal nonequilibrium coefficient η. Fig. 7 illustrates such coefficient versus the tube length to diameter ratio L/D at inlet saturated condition, and η is linearly correlated as

$$N = 0.037 \cdot L/D - 0.164 \tag{6}$$

The exit thermal nonequilibrium coefficient for subcooled inlet condition is different from that of saturated inlet condition. At higher inlet liquid subcooling, the flow should cover a longer distance for the liquid reaching the saturated condition. Further pressure decrease along the flow direction may cause the flashing process between the two phases. In other words, at subcooled inlet condition, the flashing process can not occur easily than that for saturated inlet condition. Thus less vapour is produced and eventually induce a higher critical mass velocity. Based on this analysis, N in Eq. (6) should be modified to take account of the inlet subcooling effect. Such modification is written as

$$N = [0.037 \cdot L/D - 0.164]\exp\left[-20.7\left(\frac{\Delta T_{sub}}{T_c}\right)\right] \tag{7}$$

where T_c is the critical temperature. The value is 647.27 K for water. From Eq. (7) we see that the modification coefficient is less than unity.

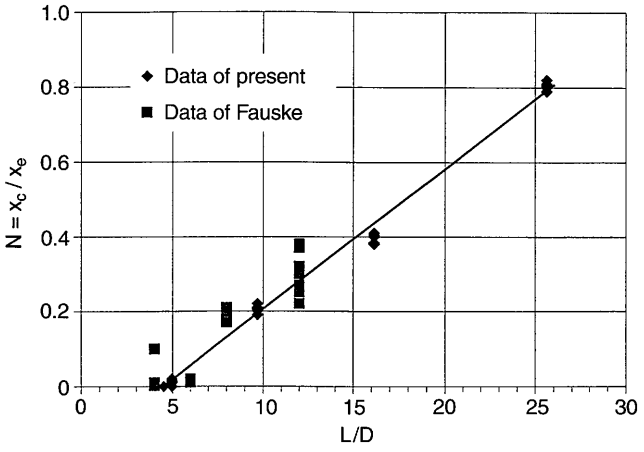

Fig. 7. Non equilibrium coefficient versus L/D

Up to now, the critical mass velocity can be acquired easily. This process is summarized as:

1. At the given upstream physical properties (P_o, T_o), and the tube geometries L, D, η is predicted from Eq. (4). Thus the exit pressure P_c is obtained from the inlet pressure P_o multiplying by η.
2. The thermal equilibrium vapour mass fraction x_e is calculated from Eq. (5), and the nonequilibrium coef-

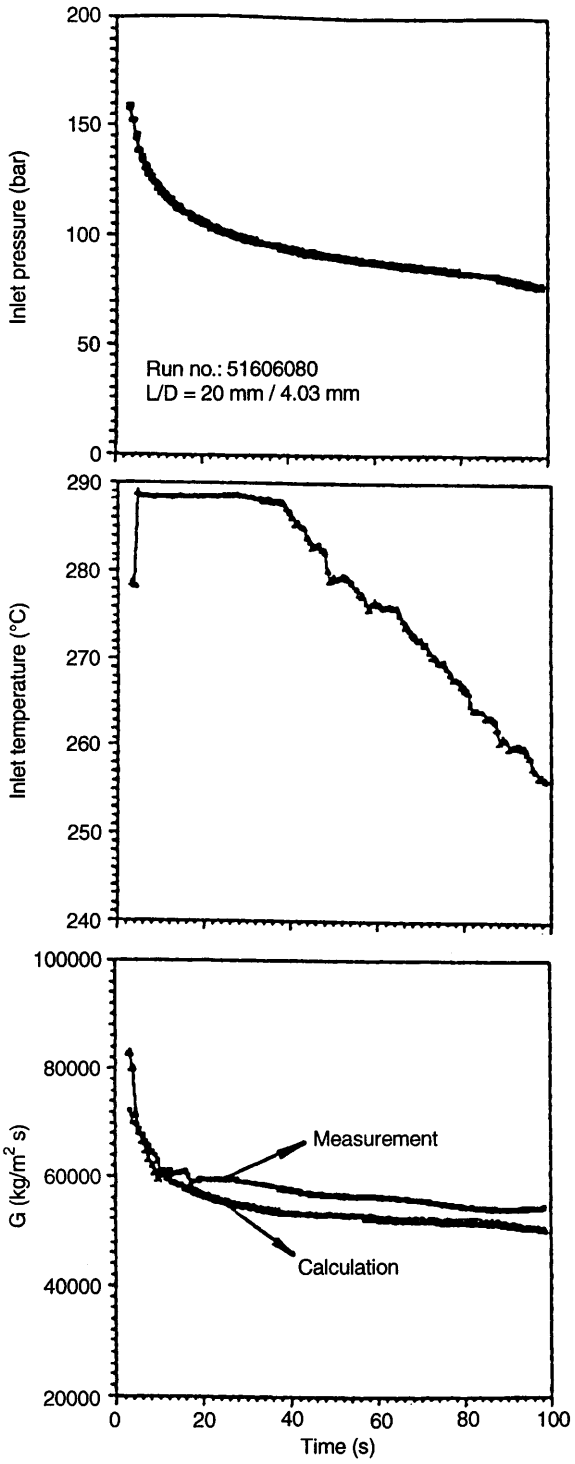

Fig. 8. Comparisons of the calculated critical mass velocity with the experimental data

ficient N is from Eq. (7). The true exit vapour mass fraction x_c is calculated from x_e multiplying by N.

3. From Eq. (2), critical mass velocity is eventually developed.

In the above process, two special conditions should be considered and they are emphasized as follows:

Orifices or short tubes consideration

Equation (7) clearly showed that N would be less than zero when L/D was less than 4.4. This demonstrated that no flashing would occur at this condition. The critical mass velocity could be easily determined by $G = 0.61\sqrt{2\rho_l P_o(1-\eta)} \cdot \eta$ was determined from Eq. (4).

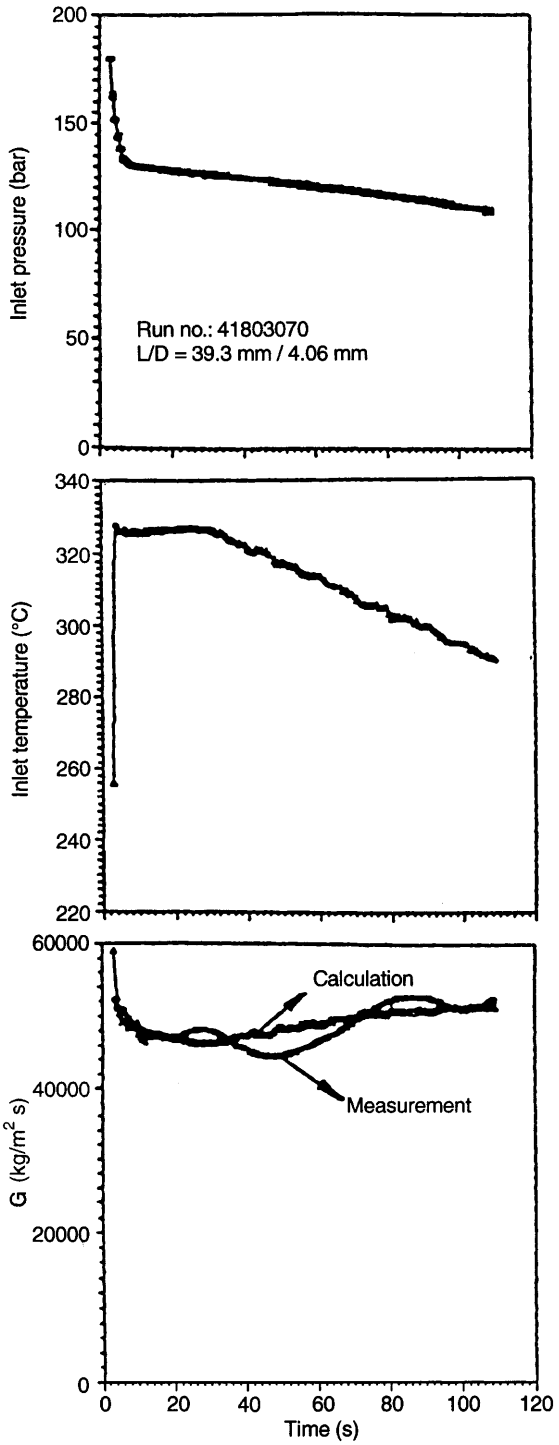

Fig. 9. Comparisons of the calculated critical mass velocity with the experimental data

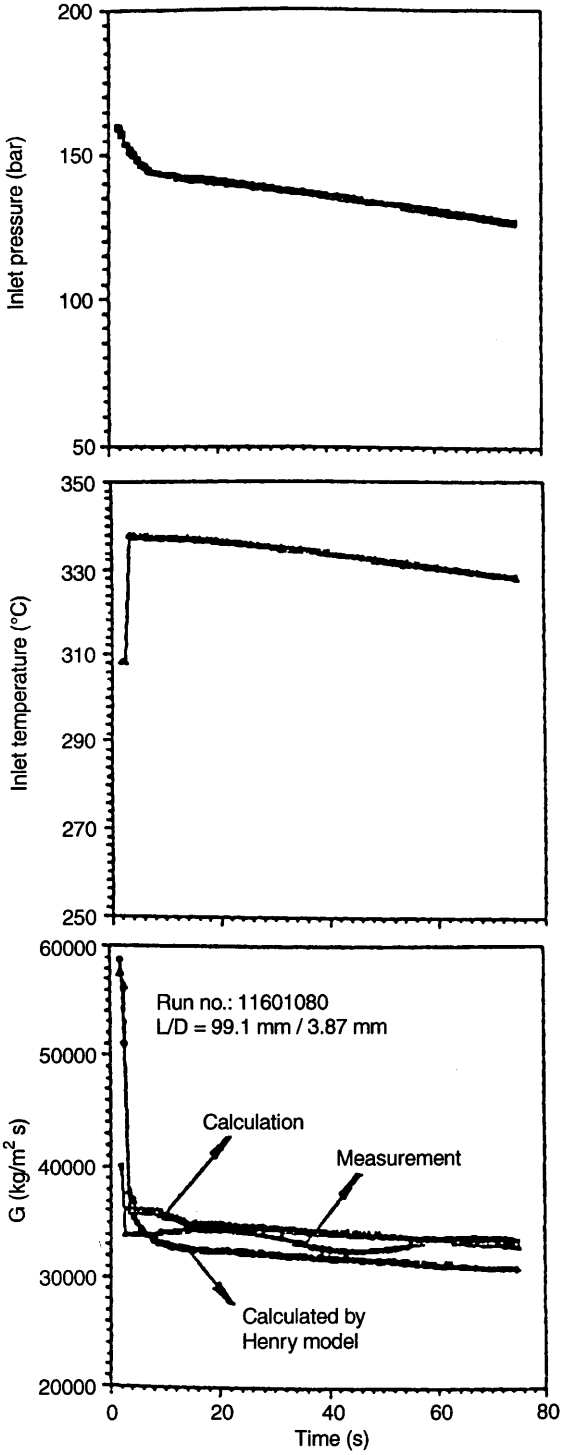

Fig. 10. Comparisons of the calculated critical mass velocity with the experimental data

Long tube and higher upstream subcooling conditions

At higher inlet liquid subcooling conditions, the calculated exit equilibrium vapour mass fraction x_e from Eq. (5) may be less than 0. This means that the saturated liquid state at the tube exit can not be reached because the pressure drop across the whole tube is not enough. The critical mass velocity can be written as

$$G = 0.61\sqrt{2\rho_l(P_o - P_c)} \tag{8}$$

From our experiment, P_c in Eq. (8) being replaced by $P_{sat}(T_o)$ only induces the maximum error of 5%.

Comparisons with the experimental data

Totally we have conducted 288 test runs based on the combinations of the initial pressure and temperature. A test run case began when the steady system pressure and the liquid temperature entering the pressure vessel were reached the desired values. Before a test run was over, the pressure vessel had a certain value of the liquid level. Thus the vapour in the top part of the vessel can not be pulled through the break tube. Generally the discharge time for most cases was nearly 2.0 minutes. The initial pressure was up to 22.0 MPa and the liquid subcooling covered the range of 0 to 60°C. The data acquisition system recorded the transient parameters, such as the break tube upstream pressure, temperature. The measured critical mass velocity was obtained from the two load cell mass with respect to time. The technique was described before. Comparisons of the correlation with the present experimental data are typically illustrated in Figs. 8–10. From these figures, it is shown that reasonable good agreement was obtained between the correlation and the measured values. The largest relative error is less than 10.0%.

Among these figures, Fig. 10 illustrates the comparisons between the correlation and the measured values for break tube section $L/D = 25.61$. Because the break tube length to diameter ratio is larger than 12, the critical mass velocity could also be predicted by Henry [16] model. The authors found that both the present correlation and the Henry model can predict the critical mass velocity. However, the present correlation is much more closer to the measured values than the Henry model predictions.

The present correlation is mainly based on our experimental data with water flowing in small diameter tube. However, the validity is also applicable to other single-component two-phase mixtures with low liquid viscosity and non-retrograde behavior.

Conclusions

1. The transient experiments with high-pressure water flowing in small diameter sharp-edged tubes were conducted. The pressure was up to 22.0 MPa and the liquid subcooling covered the range of 0 to 60°C. The break tube sections had nearly 4 mm inside diameter, but quite different lengths.
2. The present paper correlated the ratio of the exit pressure to the inlet pressure, and it was found that for longer tubes, the ratio gets nearly the same value of 0.55.
3. The paper deduced the thermal nonequilibrium coefficient from the experiment, which showed the degree at which the equilibrium state between the two phases can be reached. At higher inlet subcooling condition, such coefficient gets smaller values to lead higher critical mass velocity.
4. For orifices or very short tubes, the liquid flashing across the channel can be neglected. The critical mass velocity can be calculated from $G = 0.61\sqrt{2\rho_l(1-\eta)P_o}$, η is from Eq. (4).
5. At higher inlet liquid subcooling and longer tubes, if the calculated exit equilibrium vapour mass fraction is less than zero, we conclude that the single-phase flow may cover the whole tube. The critical mass velocity can be predicted by Eq. (8), and the exit pressure being replaced by $P_{sat}(T_o)$ only introduces small error.
6. The advantage of the present correlation is that it needs less time to perform the calculations.

References

1. **Isbin HS; Moy JE; Dacruz JR** (1957) Two Phase Steam Water Critical Flow. AICHE J 3: 361–365
2. **Fauske HK** (1962) Contribution to the Theory of Two-Phase, One-Component Critical Flow, ANL-6633
3. **Zaloudek FR** (1961) The Low Pressure Critical Discharge of Steam-Water Mixtures from Pipes, Hanford Atomic Products Operation Report, HW-68934, Rev
4. **Faletti DW; Moulton RW** (1963) Two-Phase Critical Flow of Steam-Water Mixtures. AICHE J 9: 247–253
5. **James R** (1962) Steam-Water Critical Flow through Pipes, Procedings of the Institution of Mechanical Engineers, Thermodynamics and Fluid Mechanics Group 176(26): 741–748
6. **Zaloudek FR** (1963) The Critical Flow of Hot Water through Tubes, Hanford Atomic Products Operation Report, HW-77594
7. **Zaloudek FR** (1964) Steam-Water Critical Flow From High Pressure Systems, Hanford Atomic Products Operation Report, HW-80535
8. **Fauske HK** (1965) The Discharge of Saturated Water through Tubes, Chemical Engineering Progress Symposium Series 61(59): 210–216
9. **Sozzi GL; Sutherland WA** (1975) Critical Flow of Saturated or Subcooled Water at High Pressures, ASME Symposium, Vol. Nonequilibrium Two-Phase Flows, pp. 19–25
10. **Hutcherson MN** (1975) Contribution to the Theory of the Two-Phase Blowdown Phenomenon, ANL-75-82
11. **Ardron KH** (1978) A Two-Fluid Model for Critical Vapour-Liquid Floq. Int J Multiphase Flow 4(3): 327–337
12. **Richter HJ** (1983) Separated Two-Phase Flow Model: Application to Critical Two-Phase Flow. Int J Multiphase Flow 9(5): 511–530
13. **Elias E; Chambe PL** (1984) A Mechanistic Nonequilibrium Model for Two-Phase Critical Flow. Int J Multiphase 10(1): 21–40
14. **Dobran F** (1987) Nonequilibrium Modeling of Two-Phase Critical Flow in Tubes. ASME J Heat Transfer 109: 731–738
15. **Shin TS; Jones OC Jr** (1986) An Active Cavity Model for Flashing. Nuclear Eng Design 95: 185–196
16. **Henry RE** (1970) The Two-Phase Critical Discharge of Initially Saturated or Subcooled Liquid. Nuclear Science and Engineering 41: 336–342